2019 IEEE 15th International Conference on Automation Science and Engineering (CASE)

Iterative learning control for power profile shaping in selective laser melting

Aleksandr Shkoruta, William Caynoski, Sandipan Mishra, Stephen Rock

***Abstract*— Selective laser melting (SLM) can be used to manufacture functional metal parts with complex geometries that cannot be produced by traditional manufacturing methods. However, SLM process control cannot yet guarantee the end part quality required for critical applications. The application of model-based control strategies to SLM is complicated by both the closed architecture of industrial SLM machines and the lack of suitable control-oriented process models. In this paper we (1) present an open-source SLM printer that allows implementation of the on-the-fly power adjustment and (2) use a data-driven method, iterative learning control (ILC) to learn the suitable laser power profile using the melt pool emission measurements from a coaxial camera. We demonstrate the effectiveness of the proposed ILC approach through experiments on the open-source SLM machine.**

I. INTRODUCTION

Additive manufacturing (AM) is an umbrella term for a variety of manufacturing technologies that work by gradually adding material to a part being built in a layer-by-layer fashion. ASTM categorizes 7 families of the AM processes, powder bed fusion (PBF) being one of them [1]. One type of such PBF process employs a high-power laser to melt and fuse metal and is known as selective laser melting (SLM). In the SLM process, a recoater spreads a thin layer of metal powder over the build plate. The laser scans this metal powder, which locally melts and then solidifies. The build plate is then lowered, and the recoater spreads a new layer of powder on top of the just melted material. To focus the laser onto a precise location on the build plate, a combination of a lens and a computer-controlled scanner is commonly used. Fig. 1 illustrates a schematic of a generic SLM machine.

SLM promises unprecedented flexibility in the design of fully-functional metal parts. However, high thermal gradients and cooling rates inherent to the process frequently cause defects such as thermally-induced deformations, porosity, and cracks [2]. Currently, process parameters to achieve the desired end part quality are determined by trial-and-error, with power level kept constant within predefined scan segments.

This work is supported by NSF Data-Driven Cyberphysical Systems Award #1645648 and by the State of New York ESD/NYSTAR program. All opinions, results, findings and/or interpretations presented here are those of the authors and do not necessarily represent those of the State or Federal funding agencies.

Aleksandr Shkoruta, William Caynoski, Sandipan Mishra are with Department of Mechanical, Aerospace, and Nuclear Engineering, Rensselaer Polytechnic Institute, Troy, NY 12180, USA. Stephen Rock is with Center for Automation Technologies and Systems, Rensselaer Polytechnic Institute, Troy, NY 12180, USA. shkora, caynow, mishrs2, rocks@rpi.edu

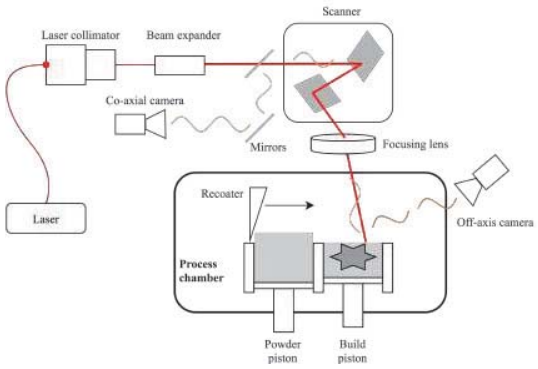

Fig. 1. Generic SLM machine diagram showing a laser, laser delivering optics, and contents of a process chamber. Darker gray depicts a solid part, while lighter shade shows unmelted powder. Each layer, the powder piston moves upwards to supply the recoater with fresh powder. Simultaneously, the build piston lowers so a new powder layer can be spread onto the part.

Implementation of other power control strategies is complicated for several reasons. First, industrial SLM printers do not allow adjusting the power within a single scan line. Second, there is the lack of the control-oriented SLM process models, with existing finite element models being extremely computationally demanding [3]. Last, in-situ measurement of SLM process is also challenging, even though significant breakthroughs were reported recently [4].

As a result, reported control strategies for SLM are limited, even though feedback control of AM processes in general has seen significant interest [5]. The seminal work in SLM control to date is the PID controller presented in [6]. One approach to circumvent modeling issue is to use in-situ process measurements in combination with model-free data-driven control methods to improve process performance.

In this paper, we experimentally investigate the use of a model-free design approach to laser power control in SLM. Using our in-house built open-source machine, we command a power profile that varies *within scan segments*, based on in-situ coaxial camera measurements. We use a feedforward data-driven control method, namely iterative learning control (ILC), to update the commanded power profile for a single part layer. ILC is a control method frequently used in the high-precision motion control [7]. We experimentally show the applicability of the selected control approach to the SLM process.

The paper is structured as follows: the problem of controlling a non-uniform process signature is mathematically formulated in Section II. We introduce iterative learning control (ILC), and motivate its application to our problem,

978-1-7281-0356-3/19/$31.00 ©2019 IEEE

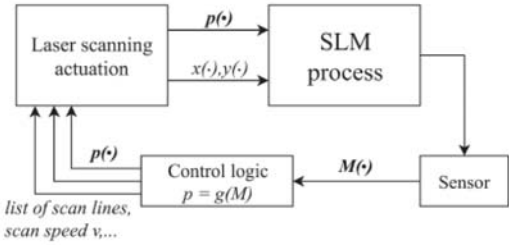

Fig. 2. The setup of the control problem. Signals of interest are in bold.

in Section III. The experimental SLM setup that allows us to change power within a single scan line is described in Section IV. Section V describes experimental design. We report results of the ILC application to SLM control in Section VI and conclude with future work in Section VII.

II. PROBLEM STATEMENT

Consider the scenario where the laser scans the powder bed along the predefined trajectory. Let $\{t_i, i = 1, 2, \dots, N\}$ be discrete time instants, where t_N is the time it takes to scan the whole cross-section. Define discretized laser power profile as $\tilde{P} = [p(t_1), ..., p(t_N)]$, where $p(t_i) \in [p_{min}, p_{max}]$ $\forall i$, and p_{min}, p_{max} are the lower and the upper limits of the achievable laser power, respectively.

Furthermore, suppose $M \in \mathbb{R}_+$ denotes a process output. For example, it could be a maximum melt pool temperature or another process signature. Discretized measurement profile over the entire scan is then $\tilde{M} = [M(t_1), ..., M(t_N)]$. Suppose that a target level for this signature is a profile $\tilde{M}_d$.

We seek the power profile $\tilde{P}^*$ such that error $\tilde{e}$ between $\tilde{M}$ and $\tilde{M}_d$ is minimized in the sense of l_2-norm:

$$\begin{aligned} &\tilde{e} \triangleq \tilde{M}_d - \tilde{M} \\ &J \triangleq \frac{1}{2}\|\tilde{e}\|_2^2 \equiv \frac{1}{2N}\sum_{i=1}^{N}(M_d(t_i) - M(t_i))^2 \\ &\tilde{P}^* = arg\min_{\tilde{P}} J \\ &\text{such that } \forall i\ p(t_i) \in [p_{min}, p_{max}] \end{aligned} \tag{1}$$

Equation (1) then defines the power profile to force signature M towards the desired level all over the part cross-section.

III. ITERATIVE LEARNING CONTROL

The control problem from Section II is a generic optimization problem. Given the full knowledge of the relationship between measurement $M(t)$ and power input $p(t)$ (i.e. white-box model), we can find optimal control input $\tilde{P}^*$ using well-established optimization methods. For example, we could use a gradient descent search:

$$\begin{aligned} &\nabla_{\tilde{P}} J = (\nabla_{\tilde{P}}\tilde{e})^T\tilde{e} \\ &\tilde{P}_{k+1} \leftarrow \tilde{P}_k - \eta\nabla_{\tilde{P}} J = \tilde{P}_k - \eta(\nabla_{\tilde{P}}\tilde{e})_k^T\tilde{e}_k \end{aligned} \tag{2}$$

where η is the learning rate (or step size), k is the step number, and $\nabla_{\tilde{P}}\tilde{e}$ is the properly defined Jacobian.

As was mentioned earlier, modeling of the SLM process is challenging. Consequently, we do not have a reliable and simple way to calculate the error gradient with respect to the commanded power profile. In the absence of the white-box model, we resort to data-driven approaches to approximate $\nabla_{\tilde{P}}\tilde{e}$. Iterative Learning Control (ILC) is one such approach.

The underlying idea behind ILC results from the fact that many manufacturing processes (including SLM) are repetitive in some form and go through same "tasks" (trials, iterations) with predictable (though unknown) disturbances. For example, a positioning system might go through the same motions run after run after run and encounter the same straightness errors at the same places on the motion guides. These repetitive disturbances manifest themselves in the output error. Therefore, outcomes of past process iterations hold the information about those disturbances. Essentially, ILC uses input-output data from past iterations to shape the input for the current iteration, i.e.

$$\tilde{u}_{k+1} = f(\tilde{u}_k, \tilde{e}_k)$$

where $\tilde{u}_k \in \mathcal{U}$ is the input profile that was fed into the plant at the iteration k, $\tilde{e}_k \in \mathcal{M}$ is the deviation of the observed output profile from the target profile at the same iteration, and $\tilde{u}_{k+1} \in \mathcal{U}$ is the input profile that will be used at the next iteration $k+1$. $\mathcal{U}$ and $\mathcal{M}$ denote the feasible input and output sets, respectively.

Several applications of ILC to AM processes are reported in the literature: ILC for selective laser sintering (SLS) of polymers in [8], and ILC for the directed energy deposition of metals in [9], [10]. Of particular relevance is the ILC law applied to SLM by Spector et al. [11]. They considered a reduced-order model of the SLM process based on heat balance equations (with conduction and convection) without melting. The objective was to find the input power profile to drive the temperature signature to a desired one. *In effect, [11] showed that it is possible to drive the process output to the desired level by adjusting the laser power using the proportional ILC update law*

$$\tilde{u}_{k+1} = \tilde{u}_k + L\tilde{e}_k, \tag{3}$$

where $L \in \mathbb{R}$ is called the learning gain. Specifically, they proved that if there exists a power profile $\tilde{P}_d$ such that the resulting temperature profile $\tilde{T} \equiv \tilde{T}_d$, then $\tilde{P}_k \to \tilde{P}_d$ if $0 < L < L_{max}$ for update law (3). Here, L_{max} depends on the material properties and the laser power distribution over the powder bed.

Comparing (3) with (2), we can observe that (3) approximates the true Jacobian of the error with a constant. Generally, such substitution is not guaranteed to converge, but we can rely on theoretical results from [11] to assume that ILC law (3) will converge if the learning gain L is sufficiently small.

Thus, in this paper, we experimentally investigate if the ILC law (3) can be used to find the power profile $\tilde{P}^*$ from (1).

IV. OPEN-SOURCE SLM MACHINE TEST BED

We evaluate the ILC learning law as an approach to solve the problem (1) experimentally on an open source SLM

machine built in-house at Rensselaer Polytechnic Institute (RPI) in Troy, NY. The test bed used for this study is shown in Fig. 3. The list of primary components is summarized in Table I. The architecture of the system can be decomposed into the following subsystems:

1) The laser beam delivery subsystem
2) Process chamber with the controlled atmosphere
3) Powder delivery & the build plate actuation subsystem
4) Process monitoring & sensors
5) Control software & GUI.

We now briefly discuss each of these parts.

1) Laser beam delivery: The laser beam is delivered to the build plate through the following: a laser collimator, a beam expander, a scanner, and a $f\theta$ lens. The collimator is the standard one supplied by the laser manufacturer. The beam expander is used to widen the laser beam so it gets focused into a smaller laser spot on the build plate. The galvanometer scanner head is the 2-axis system designed specifically for the laser processing applications. The $f\theta$ lens is the lens that is specifically designed to provide flat focusing surface, unlike standard focusing lenses.

2) Process chamber: A repurposed vacuum chamber works as the process chamber in our case. For each build, the chamber is vacuumed down and then back-filled by an inert gas (Argon) to prevent oxidation of the powder and avoid fire hazard.

3) Powder delivery and the build plate actuation: The build plate supports parts with up to 50×50 mm cross-sections. Both the build piston and the powder piston are actuated by the servomotors located outside of the process chamber. To spread the powder over the build plate, a silicone blade recoater is used. The recoater motor sits outside of the process chamber and couples to the recoater via a magnetic coupling through the chamber wall, a worm gear, and a chain drive.

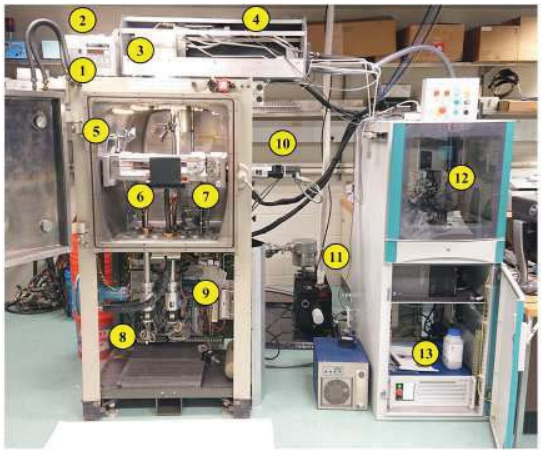

Fig. 3. Open-source SLM machine. *1* - oxygen analyser, *2* - off-axis camera (not visible), *3* - scanner, *4* - coaxial camera, *5* - mirrors for the off-axis camera, *6* - dust collector, *7* - recoater, *8* - powder piston (left) and build platform piston (right), *9* - motion controller, *10* - recoater drive, *11* - roughing pump, *12* - industrial PC cabinet, *13* - laser.

Fig. 4. A sample part produced on the SLM test bed (post-processed).

4) Sensors: The machine currently employs two sensors for in-situ process monitoring and real-time sensing: a thermal camera overlooking the whole build area (referred to as the "off-axis"), and a near-infrared camera looking at the build area through the laser focusing optics (referred to as the "coaxial").

The off-axis thermal camera (FLIR model A320) observes the whole build area through a vacuum viewport. The instantaneous field of view (IFOV) of the camera is 1 mm per pixel, with a frame-rate of 60 Hz.

The coaxial camera (Thorlabs model DCC3240N) is used to observe the melt pool area. The optical setup is similar to the ones reviewed in literature [4], [5]. Process emissions from the melt pool area are transmitted through the laser focusing optics, are redirected by a long-pass beam splitter and a folding mirror towards the camera, and are focused by an achromatic lens in combination with an extension tube. The resulting system has IFOV of 21 microns per pixel. Therefore, depending on process conditions, the melt pool width is 5 or more pixels. To increase the temporal resolution of the sensor, we limit the camera's region of interest and achieve frame rates up to 800 Hz. By design (i.e. use of the

TABLE I
EQUIPMENT LIST

Laser	IPG Photonics 1070 nm $40 - 400$ W power range
Beam expander	Sill Optics S6EZM5076/328 motorized, up to $8\times$ magnification
Scanner	SCANLAB intelli$SCAN_{de}$ 20 typical marking speed 1 m/s step response (1% full scale) 0.7 ms
Focusing lens	Sill Optics S4LFT1420 focal length 420 mm nominal spot $\varnothing 60$ μm ($\varnothing 14$ mm beam)
Off-axis imaging	FLIR A320 waveband $7.5 - 13$ μm 320×240, 60 Hz
Coaxial imaging	Thorlabs DCC3240N filter waveband 880 ± 35 nm FWHM 40×40 subwindow, 800 Hz
Scanner controller	SCANLAB RTC5 PCI control board
Motion controller	Galil DMC-4080

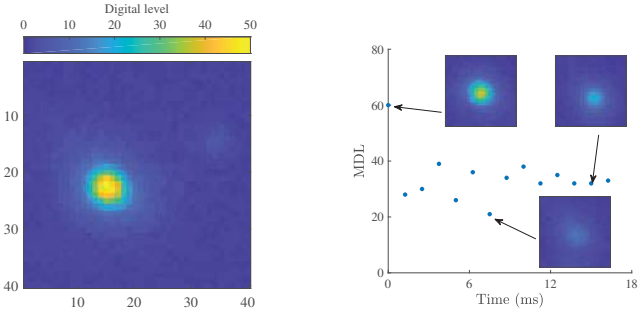

(a) (b)

Fig. 5. (a) Example of a coaxial image (false color). (b) Example evolution of the MDL signal within a single scan line.

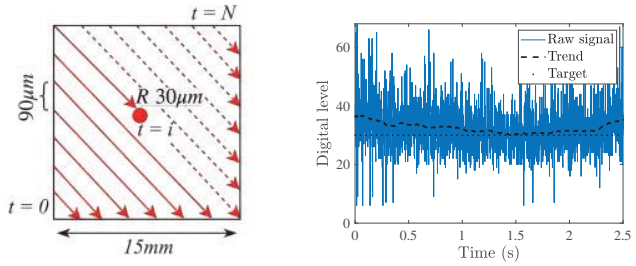

(a) (b)

Fig. 6. (a): scan pattern in our test. The red circle shows a snapshot of the laser location, while the solid and the dashed lines represent segments already scanned and to be scanned, correspondingly. Hatch spacing and laser spot size not to scale. (b): coaxial process signature (MDL) for the open-loop scanning of the test layer geometry. The bowl-shape trend is clearly visible in the filtered signal. Trend is extracted using moving average filter, window size 200.

same scanner mirrors for both laser scanning and process observation), the camera's FOV always follows the heat-affected zone, thus subwindowing of the camera does not limit the machine's workspace.

5) Control software & GUI: All the different hardware components of the system, from the laser to the recoater motor to the sensors are synchronized and controlled using LabVIEW interface contributed by America Makes [12]. Communication with the laser and the scanner is performed from within LabVIEW interface using RTC5 control board API. When a part is being built, LabVIEW code reads layer scan files and repeatedly sends lists of scan lines to the scanner. Additionally, for each layer, the coaxial measurements are acquired using a software trigger and are stored in RAM. Once a layer is completed, those images are saved to a hard drive.

V. EXPERIMENT DESIGN

We elaborate upon exact details of the experimental evaluation of the ILC algorithm 3 in the following subsections.

A. Process signature, M

The coaxial camera provides us with a 2D intensity image $I(x, y)$ (Fig. 5a) each time t_i it is triggered. Several alternative signatures can be extracted from such an image.

It is widely believed that the maximum melt pool temperature is an important contributor to the end part quality. If the coaxial image is treated as a proxy for the temperature distribution in the proximity of the melt pool, we believe that temperature convergence guarantees established in [11] can be extended to the brightness of the coaxial images. Therefore, we selected the maximum digital level (MDL) as the process signature M:

$$M = MDL(t_i) = \max_{x,y} I(x, y, t_i)$$

Example MDL data with corresponding coaxial images is given in Fig. 5b.

B. Test layer geometry

We chose a square cross-section with a diagonal scan pattern (shown in Fig. 6a) as the test case in this study. Such scan sequence is standard for producing SLM parts. The side length of the pattern was equal to 15 mm, and scan speed was kept at 600 mm/s. Nominal open-loop power level was set to 250 W[1]. This was the constant power sent for the first ILC iteration $k = 0$. We repeated diagonal scan pattern for iterations $k = 1, 2, ...$ and updated commanded power profile based on the coaxial measurements. The sampling time for updating laser power was set to 1.25 ms to match the coaxial data acquisition rate.

MDL for the open-loop layer scanning of the scan pattern in Fig. 6a is shown in Fig. 6b. We set the learning gain L and the target level $\tilde{M}_d$ based on this measurement. Short scan segments at the corners (in the beginning and at the end of the scan) cause the local change in the coaxial process signature M. As the measurement is very noisy, we only show the filtered version of the coaxial data (with filter always stated in the caption) from now on.

C. Target output profile

To enforce uniformity across all scanned locations, the target profile $\tilde{M}_d$ was chosen to be a constant M_d. From Fig. 6b, we chose $M_d = 30$. In general, the target profile $\tilde{M}_d$ should envelop the notion of "good" part quality, and should be selected accordingly (e.g. to get suitable melt pool size, grain size, or other desired outcome, based on trial-and-error or appropriate simulations). In this paper, we assume that target profile is properly selected, and the problem of ensuring print quality is equivalent to the problem stated in Section II.

D. ILC update law

We limited the laser power level to values between 190 W and 310 W based on safety and hardware constraints. Thus, ILC update law was set to

$$\tilde{P}_{k+1} = Sat_{[p_{min}, p_{max}]}\left(\tilde{P}_k + L\tilde{e}_k\right) \quad (4)$$

where index k denotes the iteration number, and Sat represents point-wise profile saturation, i.e. out-of-bounds values

[1]It should be noted that all powers mentioned in this section are the nominal commanded values. The actual power that reaches the powder bed is smaller due to the losses in the optical path.

are reset to the corresponding boundary value. As before, $\tilde{e}_k \equiv [M_d - M_k(t_1), M_d - M_k(t_2), \ldots, M_d - M_k(t_N)]$.

We selected the learning gain L heuristically: as the span of the coaxial signature M was around 60, and the power was constrained to 250 ± 60 W, a reasonable estimate for the learning gain was $L \approx 1$ Watt per digital level. We started with a conservative choice of $L = 0.2$ and then transitioned to $L = 2$ once it was established that $L = 0.2$ does not cause any adversarial effects. In this paper, we seek to prove that there exists *some* learning gain that will work with ILC law 4. Selection of the *optimal* learning gain, or establishing the convergence bounds, are out of the scope of this paper and are subject of the future work.

The coaxial signature M clearly has high frequency fluctuations. Therefore, (4) can result in a noisy power profile. One way to address this is to use a filter, which is a common practice in ILC [7]. If we denote low-pass filtering operation as $Q : \mathcal{U} \to \mathcal{U}$, then ILC update (4) takes the form

$$\tilde{P}_{k+1} = Sat_{[p_{min}, p_{max}]}\Big(Q\big[\tilde{P}_k + L\tilde{e}_k\big]\Big) \tag{5}$$

We have run the tests with and without low-pass filtering (i.e. $Q \equiv 1$ and Q being moving average filter with window size 50) and with two different values of gain L. The results from these tests are described in the following section.

VI. Results

A. Lower gain $L = 0.2$, no Q-filter in ILC law

We implemented ILC for 10 iterations (i.e. repeated diagonal square scans 10 times), and observed that power profile changed the trend of M to track M_d. Thus, with the use of (4), the systematic bowl-shape trend observed in the coaxial process signature was removed.

From the observation of unfiltered error profiles, it was clear that while the error span did not decrease, the mean level error disappeared. This is to be expected as ILC can only remove repeating (systematic) sources of error. Since the error profiles were very noisy, to quantify the rate of ILC convergence (if any), we filtered the error profiles using a moving average (as in Fig. 6b), and used the norm of the resultant filtered error profile $F(\tilde{e})$ as the measure of ILC success. Filtered error profiles for a number of iterations are shown in Fig. 8 (left), and the evolution of corresponding norm is shown in Fig. 8 (right). Using (4), high frequency components in $\tilde{e}_k$ propagated to the commanded power profile, as clearly visible in Fig. 7. However, once the trend in power profiles was extracted, steady development towards dome-like shape was observed. As the commanded power profiles were very noisy, we chose not to analyze the convergence of their norms.

Based on the above results, it was evident that the application of a Q-filter was necessary to limit the propagation of the high-frequency components of the coaxial MDL signal to the commanded power profile. We also increased the gain L, as the value of 0.2 appeared to lead to comparatively slow convergence, thus safety concerns were unwarranted.

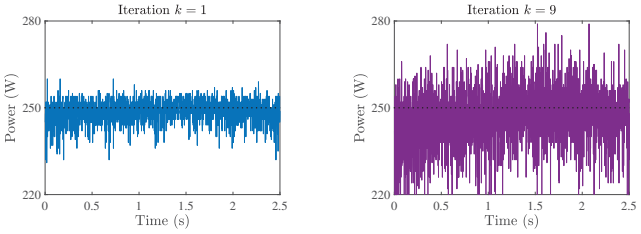

Fig. 7. Commanded power profiles, no Q-filter, iteration $k = 2$ and $k = 9$. Span of the control input drastically increased.

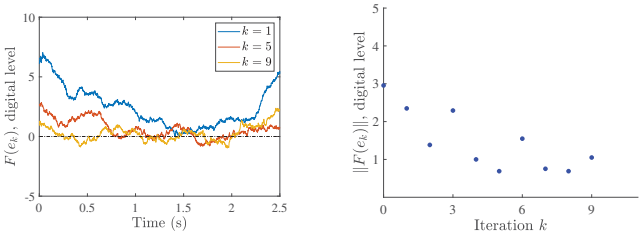

Fig. 8. Convergence of ILC law (4), for $L = 0.2$, no Q-filter. *Left:* evolution of the error profile trend. To get the trend, error profiles are aggressively post-processed with moving average filter, window size 200. *Right:* Evolution of the norm of the filtered error profile with iteration. Fluctuating downward trend is clearly visible, which aligns with observation of error profiles themselves.

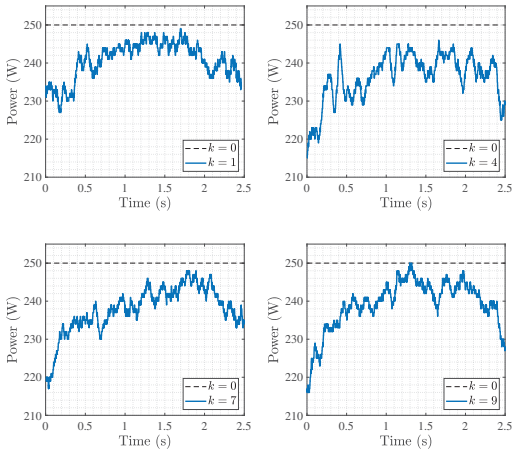

Fig. 9. Commanded power profiles for selected iterations, $L = 2$ with Q-filter. Note that the smallest power increment is 1 W.

B. Higher gain $L = 2$, moving average Q-filter

The difference between (4) and (5) lies in the use of a low-pass filter to all updates to the power profile $\tilde{P}_k$. We chose a moving average filter with window size 50 as Q. As expected, resultant power profiles were significantly smoother than in non-filtered case, and the range of commanded powers was smaller (Fig. 9).

Meanwhile, error profile shapes resembled the ones acquired with lower gain and no Q-filtering (Fig. 10). As before, the error profile exhibited large bowl-like shape in the beginning and eventually ceased to have any mean level displacement. However, the behavior of the filtered error norm was different: the decrease appeared to be smoother

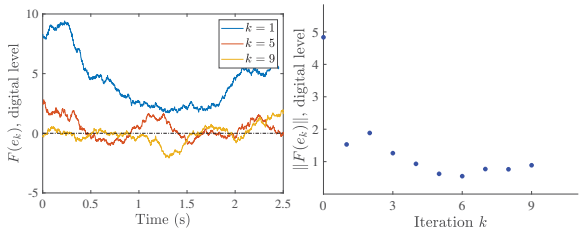

Fig. 10. Convergence of ILC law (5), $L = 2$, with Q-filter. *Left:* representative errors in M for the several iterations, filtered the same way as in Fig. 8. *Right*: convergence of the norm of the filtered error with iteration.

and sharper.

Interestingly enough, the input power profiles exhibited sawtooth-like shape, with "teeth" not necessarily aligning from iteration to iteration. This non-repetitive behavior effectively prevented further convergence of the ILC update. Less aggressive filtering of the coaxial signature M (i.e. moving average filter with window size 50 instead of 200) also showed the same sawtooth-like shape.

Naturally, large changes in the observed error cause large changes in the commanded power profile. In Fig. 11, observed error (blue) corresponds to power commanded on the next iteration (red) pretty well as the peaks and valleys align. However, the result of the next iteration (black dashed line) still has the sawtooth-like shape but "teeth" are now misplaced with respect to the original locations. Further investigation into the root cause of this behavior is outside the scope of this paper.

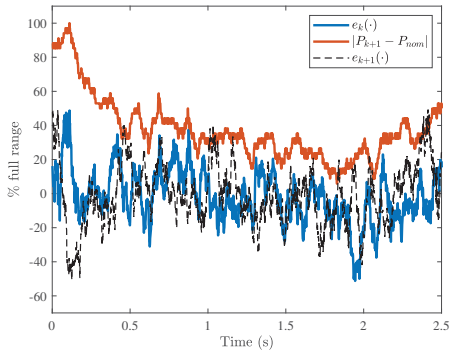

Fig. 11. Observed error $\tilde{e}_k$, subsequently calculated power profile, and resultant error $\tilde{e}_{k+1}$, scaled to their respective ranges. We plot the difference between $\tilde{P}_k$ and $P_{nom} \equiv 250\ W$. Iteration $k = 6$. Note how original error and power follow each other but subsequent error and power do not.

In summary, we have demonstrated that ILC can be used to correct systematic errors in the coaxial signature and that low-pass filtering to remove non-repetitive error components is extremely important for achieving this result.

VII. CONCLUSION AND FUTURE WORK

In general, a uniform process signature for a generic scan pattern cannot be achieved with a constant laser power level. Furthermore, the selection of the power profile is complicated due to the modeling difficulties. In this work, we have reported the successful use of the on-the-fly within-layer laser power control. We have also demonstrated that data-driven methods (for example, ILC) can be used to circumvent modeling issues and to control the process outcomes. We showed this by using ILC update law to drive an example process signature (maximum brightness of the coaxially acquired image) to the desired level for an example layer geometry. Thus, data-driven approach to the real-time SLM process control is a viable option for further investigation.

To practically apply these results, one has to note that for a whole build, following considerations become important:

1) ILC requires exact repetition of system trajectories from iteration to iteration. However, layer geometries generally do not repeat exactly.
2) Initial conditions should also repeat between iterations. But in a part with multiple layers, the state of a layer might be affected by the previous layers (due to the heat build-up, for example).

We believe that some continuity between subsequent layer scan patterns is reasonable to assume, therefore a power input profile generalization based on a learned "basis" subset could be possible. Such generalization, as well as a study of the sensitivity of our approach to the layer's initial conditions, will be the subject of the future work.

REFERENCES

[1] ASTM F2792-12a, Standard terminology for additive manufacturing technologies, (Withdrawn 2015), ASTM International, West Conshohocken, PA, 2012, www.astm.org

[2] M. Grasso and B. M. Colosimo, "Process defects and in situ monitoring methods in metal powder bed fusion: a review", *Meas. Sci. Technol.*, vol. 28, no. 4, p. 044005, 2017.

[3] M. M. Francois et al., "Modeling of additive manufacturing processes for metals: Challenges and opportunities", *Curr. Opin. Solid State Mater. Sci.*, vol. 21, no. 4, pp. 198206, Aug. 2017.

[4] M. Mani, B. M. Lane, M. A. Donmez, S. C. Feng, and S. P. Moylan, "A review on measurement science needs for real-time control of additive manufacturing metal powder bed fusion processes", *Int. J. Prod. Res.*, vol. 55, no. 5, pp. 14001418, Mar. 2017.

[5] G. Tapia and A. Elwany, "A review on process monitoring and control in metal-based additive manufacturing", *J. Manuf. Sci. Eng.*, vol. 136, no. 6, p. 060801, 2014.

[6] T. Craeghs, F. Bechmann, S. Berumen, and J.-P. Kruth, "Feedback control of Layerwise Laser Melting using optical sensors", *Physics Procedia*, 2010, vol. 5, no. PART 2, pp. 505514.

[7] D. A. Bristow and M. Tharayil, "A survey of iterative learning control", *IEEE Control Syst.*, vol. 26, no. 3, pp. 96114, 2006.

[8] A. Nettekoven, S. Fish, U. Topcu, and J. Beaman, "Predictive iterative learning control with data-driven model for optimal laser power in selective laser sintering", *29th Annual International Solid Freeform Fabrication Symposium*, Austin, TX, 2018, pp. 23272334.

[9] A. Herali, A. K. Christiansson, and B. Lennartson, "Height control of laser metal-wire deposition based on iterative learning control and 3D scanning", *Opt. Lasers Eng.*, vol. 50, no. 9, pp. 12301241, Sep. 2012.

[10] P. M. Sammons, D. A. Bristow, and R. G. Landers, "Iterative learning control of bead morphology in Laser Metal Deposition processes", *2013 American Control Conference*, Washington, DC, 2013, pp. 5942-5947.

[11] M. J. B. Spector et al., "Passivity-based iterative learning control design for selective laser melting", *2018 Annual American Control Conference (ACC)*, Milwaukee, WI, 2018, pp. 5618-5625.

[12] 4039 Development & demonstration of open-source protocols for powder bed fusion AM - America Makes. [Online]. Available: https://www.americamakes.us/portfolio/4039-development-demonstration-open-source-protocols-powder-bed-fusion-additive-manufacturing-pbfam/. [Accessed: 22-Feb-2019].